Dynamic Arrangement of Ion Pairs and Individual Contributions to the Thermal Stability of the Cofactor-Binding Domain of Glutamate Dehydrogenase from *Thermotoga maritima*†

Cristian Danciulescu, Rudolf Ladenstein, and Lennart Nilsson*

Department of Biosciences and Nutrition, Karolinska Institutet, S-141 57 Huddinge, Sweden

Received March 5, 2007; Revised Manuscript Received May 23, 2007

ABSTRACT: The dynamics of a hyperthermophilic protein fragment in a water environment, as studied by performing molecular dynamics (MD) simulations at various temperatures, is compared to the dynamical behavior of a homologous mesophilic protein simulated under identical conditions. The effects on the stability of the spatial arrangement and mobility of the charged residues in solution were quantified by calculating free energy changes upon salt bridge formation in these proteins. Electrostatic free energy terms derived from a thermodynamic cycle were obtained by solving the linearized Poisson−Boltzmann equation for a series of protein conformations generated by MD simulations and placed subsequently in a continuum solvent medium. Our results show that the ion pairs are electrostatically stabilizing in most of the cases, but their individual contributions vary significantly. The greater contribution of the charged residues to the stability of the hyperthermophilic protein as compared with the mesophilic counterpart was evidenced only by the calculations that included conformations sampled at 343 and 373 K. The "dynamic" structure of the hyperthermophilic protein fragment simulated at elevated temperatures reveals an optimum placement of the ionizable residues within the protein structure as well as the role of their cooperative interactions in promoting thermal stability. The thermodynamic properties such as electrostatic free energy differences, configurational entropies, and specific heat capacities calculated in the dynamic context of the protein structure provided new insight into the mechanism of protein thermostabilization.

Proteins from hyperthermophilic organisms, although consisting of the same amino acids as their homologues from mesophiles, have a remarkably enhanced thermal stability. Numerous studies (*1*−*6*) were dedicated to understanding the physicochemical origins of the thermal stability and suggested that a variety of factors make positive contributions, such as improved packing and hydrophobic interactions, extensive networks of hydrogen bonds (*3*, *5*, *6*), and optimized electrostatic interactions (*2*, *7*). The natural proteins may not have a single dominating mechanism of stabilization; rather, their thermal stability results from the additive effects of a multitude of local improvements. However, it has been suggested that for many hyperthermophilic proteins, which usually possess an increased number of charged residues, the electrostatic interactions play a role in enhancing thermostability (*2*, *7*−*10*). The spatial optimization of the interactions between charged residues seems to be the main determinant of the favorable electrostatic contribution to thermal stability (*2*, *7*). The role played by salt bridges in protein stability was controversial. A theoretical study by Hendsch and Tidor (*11*) found that salt bridges are in general destabilizing, and this conclusion was supported by some experimental studies (*12*, *13*). However, more recent studies proposed approaches that could reconcile the apparently destabilizing effects of salt bridges with their increased abundance in hyperthermophilic proteins (*7*, *14*−*19*).

Theoretical studies on electrostatic contributions to protein stability mainly follow the continuum electrostatic approach of Hendsch and Tidor to quantifying the electrostatic free energy contribution of various salt bridges to protein stability (*11*). Taking into consideration the effects of temperature on protein hydration, Elcock (*14*) showed that at elevated temperatures the desolvation energy paid on forming a salt bridge decreases, thus leading to a favorable contribution to stability. The results of the free energy calculations are sensitive to protein conformational details (*17*, *18*). Besides, the crystal structures used in general in these calculations may not adequately represent the proteins in solution. For these reasons, Kumar and Nussinov (*17*, *18*) included the effect of protein flexibility in calculations by selecting a range of NMR conformers to sample a significant conformational space of the protein in solution. A detailed description (*15*) of the dynamical behavior of a small thermophilic protein in solution obtained from molecular dynamics (MD)[1] simulations at various temperatures revealed a reduced level of solvation of charged side chains at elevated temperatures and suggested that large ionic networks, rather than individual

† This work was supported by the Swedish Research Council.

* To whom correspondence should be addressed. Phone: +46-8-6089228. Fax: +46-8-6089290. E-mail: lennart.nilsson@biosci.ki.se.

[1] Abbreviations: MD, molecular dynamics; SD, steepest descent; ABNR, adopted basis Newton−Raphson; rmsd, root-mean-square deviation; rmsf, root-mean-square fluctuation; tm_gdh, domain II of glutamate dehydrogenase from *Thermotoga maritima*; cs_gdh, domain II of glutamate dehydrogenase from *Clostridium symbiosum*.

10.1021/bi7004398 CCC: $37.00
Published on Web 06/29/2007

FIGURE 1: Structure-based sequence alignment of the tm_gdh and cs_gdh protein fragments. Charged residues are colored red (negative) and blue (positive). Rectangles colored magenta represent α-helices, and the light magenta rectangle is a 3_{10}-helix; the extended conformations are represented as yellow arrows.

salt bridges, provide favorable electrostatic contributions to protein stability.

Salt bridges observed in the crystal structure of a protein may break and re-form in solution, and alternative pairings of the charged residues may also occur; such fluctuations of the charged residues may play a role in thermostability and thus could help to differentiate thermophilic from mesophilic proteins. MD simulations can provide valuable descriptions of the global dynamics of proteins and their local fluctuations that could widen our understanding of the molecular basis of protein stability. In this study, we performed a detailed comparison of the dynamical behavior of two homologous protein domains to investigate the contribution of the salt bridges and ionic networks to the conformational stability. The homologous protein domains belong to the glutamate dehydrogenase from the hyperthermophilic bacterium *Thermotoga maritima* (*Tm*) and from the mesophilic bacterium *Clostridium symbiosum* (*Cs*). Glutamate dehydrogenases from these bacteria form hexamers of identical subunits (*3*). The primary structure of GluDH from *Cs* shows a level of sequence identity of 35% when compared with the GluDH from *Tm*, and the overlay of their structures shows a high degree of similarity of the secondary structure elements and their spatial arrangement. The optimal growth temperatures are 37 °C for the mesophile *Cs* and 80 °C for the hyperthermophile *Tm*. The melting temperatures of the GluDH measured from thermal unfolding experiments reach 55 °C for *Cs* and 93 °C for *Tm* (*20*). A subunit of GluDH consists of two domains separated by a deep cleft; domain I is responsible for the intersubunit interactions that direct the self-assembly of the subunits into the hexamer, whereas domain II contains the nucleotide-binding site. Domain II, which was selected for this study, contains a similar number of charged residues and is structurally very similar in the two proteins but shows a large difference in thermal stability. MD simulations of the protein fragments were performed at different temperatures to obtain information about their kinetic stability and the features of their dynamics, such as the flexibility of the protein backbone and the mobility of the amino acid side chains. Special attention was paid to the dynamics of the charged residues and their electrostatic interactions within the protein. The effects on the stability of the spatial arrangement and the mobility of the charged residues in solution were quantified by calculating free energy changes upon salt bridge formation in these proteins.

MATERIALS AND METHODS

Selected Protein Domains. Two protein domains, namely, domain II of glutamate dehydrogenase from the hyperthermophilic bacterium *Tm* and from the mesophilic bacterium *Cs*, were selected. The first protein (tm_gdh, 151 residues) consists of amino acid residues 187−337 of the primary structure of GluDH from *Tm* (*20*) (PDB entry 1b26) and was previously used as a model system in a thermodynamic study by Lebbink et al. (*21*) after they determined the X-ray structure of the isolated domain at 1.43 Å resolution; this structure was used in our study. The second protein fragment (cs_gdh, 162 residues) consists of amino acid residues 208−369 of the primary structure of GluDH from *Cs* [PDB entry 1hrd; structure determined at 1.96 Å resolution (*3*)]. The amino acid sequence to be used for the cs_gdh fragment was determined by creating a structural alignment of the tm_gdh domain with subunit A of GluDH from *Cs* and selecting the matching residues. The structural alignment was performed by using the alignment facility provided by VMD (*22*). The amino acid sequences and the three-dimensional structures of the selected proteins are presented in Figures 1 and 2, respectively. The rmsd of the backbone atoms of matching residues from tm_gdh and cs_gdh is 2.09 Å. Both proteins were used to perform molecular dynamics simulations.

MD Simulation Setup. The MD simulations were carried out using CHARMM (*23*). The molecular system was described by the CHARMM22 all atom force field (*24*). Rectangular simulation boxes were defined with dimensions of 70 Å × 59 Å × 55 Å for the tm_gdh fragment and 67 Å × 62 Å × 52 Å for cs_gdh. Each protein was placed in the center of the box and was further overlaid with equilibrated cubic boxes containing 216 TIP3 (*25*) water molecules. Water molecules with the oxygen atom lying within 2.2 Å of a protein heavy atom were removed. The resulting systems contained 7286 water molecules (tm_gdh) and 6879 water molecules (cs_gdh). Both systems were energy-minimized by 100 steps with a steepest descent (SD) method followed by 100 steps of adopted basis Newton−Raphson (ABNR) minimization. The proteins were kept fixed by harmonic constraints of 50.0 kcal mol^{-1} $Å^{-2}$. All ionizable amino acid residues were assigned the charged form. Thus, the tm_gdh fragment carries a total charge of −4, and the cs_gdh fragment carries a total charge of −2. These charges were neutralized by adding four Na^+ and two Na^+ ions, respectively, at random positions in the simulation boxes. After the sodium ions had been inserted, a new energy minimiza-

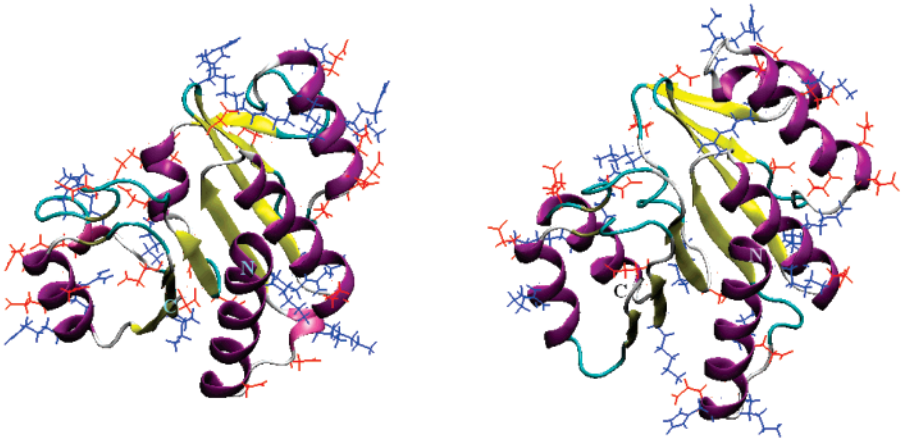

(a) tm_gdh (b) cs_gdh

FIGURE 2: Three-dimensional structure of tm_gdh (a) and cs_gdh (b). α-Helices are colored magenta, and the 3_{10}-helix is colored light magenta; the extended conformations (*β*-strands) are colored yellow. N- and C-termini are labeled N and C, respectively. Charged residues are colored red (negative) and blue (positive).

tion was performed consisting of 200 steps of SD with a 50.0 kcal mol^{-1} $Å^{-2}$ harmonic restraint on the protein fragments followed by 200 steps of ABNR minimization with the harmonic restraint decreased to 20.0 kcal mol^{-1} $Å^{-2}$. The atomic coordinates were saved after the minimization and used as initial coordinates for all further MD simulations. The MD simulations were performed using periodic boundary conditions. The initial velocities of the atoms were taken from a Maxwell distribution assigned at 50 K by using a different seed for every simulation. After the system had been heated to the temperature of interest, the simulations were continued at a constant temperature and pressure based on extended system methods (*26*−*28*) available in CHARMM. The leapfrog integration algorithm and a time step of 2 fs were used in all simulations. The bonds involving hydrogen atoms were constrained to their ideal values using the SHAKE algorithm (*29*). The nonbonded interactions were evaluated using an atom-based cutoff method with a cutoff distance of 12 Å and a cutoff of 14 Å for generating the list of atom pairs. The truncation of the long-range interactions was smoothed by a shift function (CHARMM option FSHIFT), a method that has been shown to work well also for highly charged biomolecules, such as nucleic acids (*30*). Molecular dynamics simulations for both the tm_gdh and cs_gdh systems were performed at simulation temperatures of 300, 343, 373, and 500 K.

Analyses of MD Trajectories. The dynamics and the structural changes of the protein fragments were analyzed by calculating root-mean-square deviations (rmsd) of the protein atoms, the radius of gyration, and the secondary structure of the protein as a function of time. The mobility of different residues along the protein chains was quantified by calculating the root-mean-square fluctuations of C_α atoms (standard deviation of atomic displacements) over a period of simulation time. In general, rmsd values for the backbone atoms of up to 2−2.5 Å in our simulations indicate the stability of the starting conformation as seen by visualizing the MD trajectories and by calculating the rmsd per residue; the conformational changes corresponding to this rmsd range of values would be termed "minor" conformational changes. The energy-minimized conformation (crystal structure) of either tm_gdh or cs_gdh was used as reference structure for the analyses (where needed).

The change per residue of the secondary structure with time was monitored with the "Timeline" facility of VMD, which calculates the secondary structure as defined by STRIDE (*31*). The intraprotein electrostatic interaction energy was calculated from the MD trajectories at 300, 343, and 373 K. The electrostatic interactions were evaluated using an atom-based cutoff method with a cutoff of 12 Å smoothed by a shift function. An analysis of the distance distribution of the charged residues complements the energy analysis. The distance between the charged side chains was calculated as the distance between atoms NZ (Lys), CZ (Arg), CE1 (His), CG (Asp), and CD (Glu). The charged residues were grouped into two subgroups, Pos (Lys, Arg, and His) and Neg (Asp and Glu), and three types of interacting distances were calculated: Pos−Neg, Pos−Pos, and Neg−Neg. The distance distribution comprising the interval from 0 to 60 Å was calculated from each MD trajectory over the simulation interval of 1000−4000 ps, and it was normalized in each case by dividing it by the total number of interacting pairs corresponding to the interacting subgroups. The normalized number of interacting pairs was expressed as a fraction of the total number of interacting pairs. The distances between donor and acceptor atoms of the charged residues able to form salt bridges were also monitored as a function of time.

Calculation of the Electrostatic Strength of Ion Pairs. The effects on the stability of the spatial arrangement of the charged residues in both tm_gdh and cs_gdh and of the fluctuating interaction distances between charged residues during the MD simulations were quantified by calculating the electrostatic contribution to the free energy change upon salt bridge formation in these proteins. The electrostatic contribution of an ion pair ($\Delta\Delta G_{tot}$) was calculated according to the method introduced by Hendsch and Tidor (*11*) that evaluates the contribution to the free energy of folding relative to the same protein where the side chains of a pair of charged residues are mutated to their corresponding hydrophobic isosteres (original side chains with the partial atomic charges set to zero). The folding process is decom-

posed by means of a thermodynamic cycle into "virtual" subprocesses that account for (a) the solvation and desolvation of the selected residues, (b) the "isolated" electrostatic interaction between the side chains of the selected ion pair in the folded protein, and (c) the electrostatic interaction of the ion pair with all the other partial atomic charges of the protein. The computation involves two parallel thermodynamic cycles, one with the real residues and one with the selected salt-bridging side chains mutated to hydrophobic isosteres. Thus, the free energy contributions to the stability of the protein are calculated as the difference between two corresponding ΔG values from the parallel cycles:

$$\Delta\Delta G_{tot} = \Delta\Delta G_{dslv} + \Delta\Delta G_{brd} + \Delta\Delta G_{prt}$$

where $\Delta\Delta G_{dslv}$ represents the free energy change due to the desolvation of the charged side chains when the protein undergoes the conformational change from the unfolded to the folded state (assuming that in the unfolded state the side chains are fully exposed to water), $\Delta\Delta G_{brd}$ represents the free energy due to the interaction of the two side chains with each other within the folded protein, and $\Delta\Delta G_{prt}$ represents the free energy due to the interaction of the ion pair with the rest of the protein.

The folded state of the proteins was assigned atomic coordinates obtained from the MD simulations as snapshots taken every 100 ps, after the translation and rotation of the protein had been removed. Thus, calculations were carried out using sets of atomic coordinates corresponding to different simulation temperatures (300, 343, and 373 K) to account for the dynamic structure of the protein. The unfolded state was represented as the side chain of interest alone in solution; this model assumes that the residues are separated from each other by large distances, so it neglects a possible residual structure in the unfolded state.

Electrostatic free energies were estimated from continuum electrostatic calculations performed with the Poisson−Boltzmann equation module (*32*, *33*) of CHARMM. The linearized Poisson−Boltzmann equation was solved using the successive over relaxation method. The tm_gdh protein was mapped onto a 235 × 197 × 185 grid, while cs_gdh was mapped onto a 225 × 207 × 175 grid, with the size of the grid unit cell being 0.3 Å in both cases. The partial atomic charges were taken from the CHARMM22 parameter set (*24*), and a set of atomic radii (*32*) derived from solvent electrostatic charge distribution was used. The protein−solvent boundary was defined as the molecular surface (*34*) generated with a solvent probe with a radius of 1.4 Å. The grid points within the molecular surface were assigned a dielectric constant ϵ_p of 4. The grid points outside the surface were assigned a dielectric constant ϵ_w of 80 for the calculations corresponding to a temperature of 300 K, an ϵ_w of 62 for 343 K, and an ϵ_w of 56 for 373 K, values which approximate the dielectric constant of water at these temperatures (*35*, *36*). The ionic strength was allocated a value of 0.0 M for all continuum electrostatic calculations since salt was not included in the MD simulation of these proteins either.

Calculation of the Configurational Entropy and Heat Capacity. The calculations of the entropy and heat capacity were performed using the quasi-harmonic approximation (*37*, *38*) in which the frequencies corresponding to eigenvalues

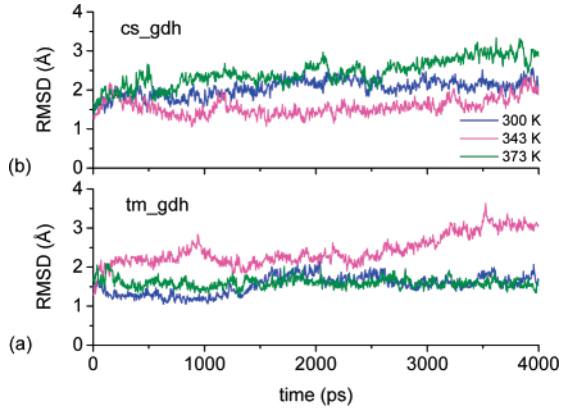

FIGURE 3: rmsds of the backbone atoms of tm_gdh (a) and cs_gdh (b) as a function of time calculated from MD trajectories at 300, 343, and 373 K.

of Cartesian covariance matrices of the positional fluctuations of the protein atoms accumulated during the molecular dynamics simulation are used in the harmonic oscillator (ho) expressions for thermodynamic quantities. Thus, for a protein consisting of n atoms, the $3n \times 3n$ mass-weighted covariance matrix is diagonalized to obtain the λ_i eigenvalues from which the quasi-harmonic frequencies are calculated as $\omega_i = (kT/\lambda_i)^{1/2}$ and subsequently substituted into the formula for entropy

$$S_{ho} = k\sum_{i}^{3n-6} \frac{\hbar\omega_i/kT}{e^{\hbar\omega_i/kT} - 1} - \ln(1 - e^{-\hbar\omega_i/kT})$$

and for heat capacity

$$C_V \equiv \frac{\partial E}{\partial T} = \sum_{i}^{3n-6} k\left(\frac{\hbar\omega_i}{kT}\right)^2 \frac{e^{\hbar\omega_i/kT}}{(e^{\hbar\omega_i/kT} - 1)^2}$$

Due to the insufficient sampling of the overall rotation and translation of the protein, these slowly converging degrees of freedom are excluded from the calculations.

The relation between the heat capacity at a constant volume (C_V) and the heat capacity at a constant pressure (C_p) is given by

$$C_p - C_V = VT\frac{\alpha^2}{\kappa}$$

where α is the "volume coefficient of expansion" and κ is the "isothermal compressibility". For proteins, as in the case of liquids and solids, the right side term is very small due to the small specific volume (V), small magnitudes, and the ratio of the expansion coefficient and compressibility. In this case, the heat capacity of the protein at a constant volume can be fairly approximated to be equal to the heat capacity at a constant pressure ($C_V \approx C_p$), and thus, our calculated heat capacities can be directly compared to the experimental values.

RESULTS

Dynamics and Stability of tm_gdh and cs_gdh Domains. rms deviations of the backbone atoms of the tm_gdh fragment as a function of time calculated from MD trajectories at 300, 343, and 373 K are presented in Figure 3a. At

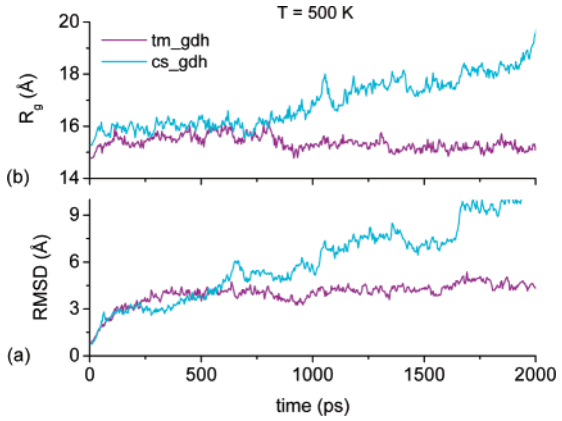

FIGURE 4: rmsds of the backbone atoms (a) and radius of gyration, R_g (b), of tm_gdh and cs_gdh as a function of time calculated from MD trajectories at 500 K.

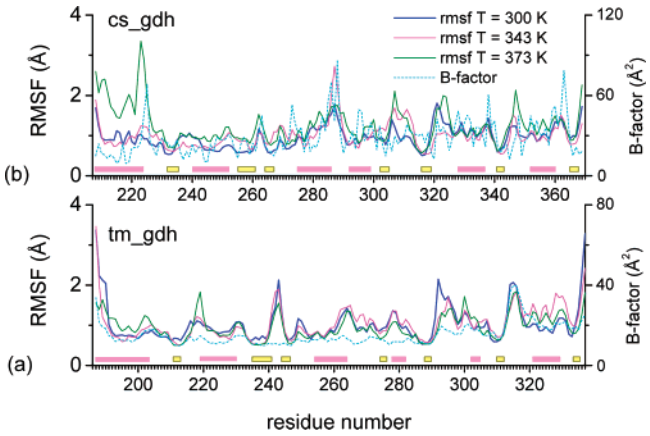

FIGURE 5: rmsfs of all atoms averaged per residue of tm_gdh (a) and cs_gdh (b) calculated over the first 2 ns of simulation, from the MD trajectories at 300, 343, and 373 K. As a reference, the *B*-factors corresponding to the protein atoms in the crystal structure are presented on the right side of the graph. The rectangles along the *x*-axis represent α-helices (magenta) and *β*-strands (yellow).

these simulation temperatures, the rmsds show steady fluctuations below 3.0 Å over the whole simulation, indicating the stability of the protein conformation. The average rmsd values calculated over the whole trajectories excluding the first 200 ps for each simulation are 1.54 ± 0.23 Å at 300 K, 2.42 ± 0.38 Å at 343 K, and 1.59 ± 0.12 Å at 373 K. A slight decrease in the rmsd is observed over the last 1500 ps of the MD simulation at 300 K with values fluctuating toward the end of the simulation around 1.8 Å. The increase in the rmsd at 343 K is due to the fraying of the marginal residues at both the N-terminus (helix H1) and the C-terminus (strand *β*7). The average rmsd values indicate minor conformational changes of the protein fragment in the simulation at 373 K.

Figure 3b presents the rmsds of the backbone atoms of the cs_gdh fragment as a function of time. At 300, 343, and 373 K, the rmsds show steady fluctuations below 3 Å over the whole simulation. The average rmsd values calculated over the whole trajectories excluding the first 200 ps for each simulation are 2.05 ± 0.21 Å at 300 K, 1.56 ± 0.22 Å at 343 K, and 2.44 ± 0.34 Å at 373 K. A slight increase in the rmsd is observed over the last part of the MD simulation at 373 K; the rmsd increases slowly and reaches ∼3 Å at the end of the simulation. At 300, 343, and 373 K, the rmsds per residue for both tm_gdh and cs_gdh indicate a larger deviation of the marginal residues at both N- and C-termini, whereas the rest of the protein remains stable.

At 500 K, the rmsd values for tm_gdh increase steadily up to 4 Å during the first 400−500 ps of the simulation and continue to increase slowly for the remainder of the simulation (Figure 4a). The end conformation of the tm_gdh fragment from the MD simulation at 500 K indicates significant changes relative to the starting structure as observed by visual inspection of the trajectory.

For the cs_gdh fragment, the rmsd increases steadily during the whole simulation at 500 K and reaches values above 10 Å after 2 ns (Figure 4a). The end conformation of cs_gdh from the MD simulation at 500 K indicates major changes relative to the starting structure.

The radius of gyration of the tm_gdh fragment as a function of time was calculated for all simulations, but only the curve corresponding to the simulation at 500 K is presented in Figure 4b. The $R_g(t)$ curves at 300, 343, and 373 K do not differ significantly; the average values of R_g corresponding to these temperatures are 14.88 ± 0.12, 14.82 ± 0.08, and 14.66 ± 0.08 Å, respectively. The radius of gyration of the starting structure is 14.75 Å. At 500 K, the radius of gyration remains stable during the simulation with an average value of 15.4 ± 0.26 Å.

The radius of gyration of the cs_gdh fragment as a function of time was calculated also for all simulations. The curve corresponding to the simulation at 500 K is presented in Figure 4b. The $R_g(t)$ curves at 300, 343, and 373 K (curves not presented) show average R_g values of 15.46 ± 0.08, 15.26 ± 0.09, and 15.43 ± 0.11 Å, respectively. The radius of gyration of the starting structure is 15.24 Å. At 500 K, the radius of gyration increases abruptly after 500 ps of simulation and reaches a peak value of ∼20 Å after simulation for 2 ns.

rms fluctuations of the atoms calculated over a MD simulation give an impression of the flexibility of the residues along the protein chain. Figure 5a presents the rms fluctuations of all protein atoms averaged per residue over the MD trajectories of tm_gdh at 300, 343, and 373 K. The data indicate a higher flexibility of residues located in regions corresponding mainly to the loops connecting the *β*-sheet and the α-helices. At 300 K, the highest rms fluctuations were observed for residues 241−244 (loop connecting strands *β*2 and *β*3), residues 261−265 (from the end of H3), residues 277−282 (helix H4), residues 291−297 (located on the loop connecting *β*5 and helical segment H5), and residues 313−319 (loop between strand *β*6 and helix H6). The marginal residues from the N- and C-termini also indicate a high flexibility which is due to the fraying of the H1 segment and distortion of the marginal *β*7 strand, respectively. The rms fluctuations of protein atoms do not show significant changes at the simulation temperatures of 343 and 373 K.

The atomic rms fluctuations per residue of the cs_gdh fragment are presented in Figure 5b. The data indicate a similar "pattern" of fluctuations as observed for the tm_gdh fragment. At 300 K, the highest rms fluctuations were observed for residues 261−263 (loop connecting strands *β*2 and *β*3), residues 282−288 (comprising the second half of helix H3), residues 305−313 (comprising a part of the loop between *β*4 and *β*5), residues 319−325 (the loop connecting *β*5 and H5), and residues 344−348 (loop between strand *β*6

Table 1: Contributions to the Intraprotein Electrostatic Energy of tm_gdh and cs_gdh Calculated from MD Simulations at 300, 343, and 373 K

interacting groups	electrostatic energy (kcal/mol) 300 K	343 K	373 K	$\Delta E_{343-300}$ (kcal/mol)	$\Delta E_{373-300}$ (kcal/mol)
tm_gdh					
Pos−Pos	−497 ± 12	−501 ± 15	−506 ± 18	−4	−9
Pos−Neg	−680 ± 41	−689 ± 77	−791 ± 94	−9	−111
Neg−Neg	84 ± 11	85 ± 15	76 ± 14	1	−8
Chrg−Nchrg	−857 ± 27	−792 ± 36	−878 ± 46	65	−21
Nchrg−Nchrg	327 ± 19	299 ± 20	306 ± 23	−28	−21
total	−1622 ± 47	−1598 ± 67	−1792 ± 83	24	−170
cs_gdh					
Pos−Pos	30 ± 12	31 ± 16	32 ± 19	1	2
Pos−Neg	−808 ± 66	−743 ± 75	−842 ± 72	65	−34
Neg−Neg	29 ± 15	10 ± 12	30 ± 13	−19	1
Chrg−Nchrg	−863 ± 26	−894 ± 28	−850 ± 32	−31	13
Nchrg−Nchrg	33 ± 21	22 ± 26	−41 ± 29	−11	−74
total	−1579 ± 68	−1573 ± 88	−1670 ± 77	6	−91

and helix H6). The rms fluctuations show a higher increase for residues 282−288 and 305−313 in the simulation at 343 K and exhibit a similar pattern for the other residues as observed at 300 K. A general increase in the atomic fluctuations is observed at 373 K along the whole cs_gdh chain. The peak values of the rms fluctuations follow the pattern observed at lower simulation temperatures.

The evolution of the secondary structure of the protein fragments was monitored for the simulations at 300, 343, 373, and 500 K. The secondary structure content is well-preserved during the simulations at 300, 343, and 373 K for both tm_gdh and cs_gdh proteins. The α-helices and β-strands exhibit remarkable stability during the whole simulation. Only marginal structural fluctuations (increasing slightly with temperature) are observed at these temperatures, mainly arising from the movement of the loops which leads to the disruption or formation of various types of turns. At 500 K, significant changes of the secondary structure were observed, especially in the cs_gdh fragment. In the tm_gdh protein, one observes distortions of the secondary structure mainly at helices H1, H2, and H4; the β-sheet core remains stable except for strand β7 (residues 333−336) which falls apart from the core and changes its conformation. The distortions of the secondary structure in the cs_gdh fragment occur at helices H1 and H4−H6 and strands β3, β4, and β7.

Energetic Analysis. Average values of the various contributions to the intraprotein electrostatic interaction energy of tm_gdh and cs_gdh were calculated from the MD trajectories at 300, 343, and 373 K and are presented in Table 1. The amino acid residues were grouped into four interacting groups, namely, positively charged residues (Pos), negatively charged residues (Neg), all charged residues (Chrg = Pos + Neg), and noncharged residues (Nchrg). The changes in the electrostatic energy contribution of the different groups as a result of the increasing temperature are reported as ΔE terms with the average energy values at 300 K as a reference.

The differences observed for the energy terms of tm_gdh as compared with the energy terms of cs_gdh are due to the different number and type of residues. Thus, considering only the charged residues, tm_gdh comprises 22 negatively charged residues (8 Asp and 14 Glu) and 18 positively charged residues (9 Lys, 7 Arg, and 2 His), whereas cs_gdh comprises 19 negatively charged residues (8 Asp and 11 Glu) and 17 positively charged residues (13 Lys, 3 Arg, and 1 His). The values of the electrostatic energy for the Pos−Pos, Neg−Neg, and Nchrg−Nchrg interacting groups contain energy terms for every residue interacting with itself (the electrostatic energy corresponding to the constituent atoms of a certain residue). The following mean values of electrostatic energy self-terms were obtained for the charged residues: 25 kcal/mol for Lys, −118 kcal/mol for Arg, 32 kcal/mol for His, 6 kcal/mol for Glu, and −12 kcal/mol for Asp. These values explain, for example, the large difference in the electrostatic energy of the Pos−Pos interactions in tm_gdh and cs_gdh; after the self-terms have been subtracted, the energy of the Pos−Pos interactions is on the same magnitude in both proteins (30−40 kcal/mol). However, the changes observed in these energy terms due to an increase in temperature are more meaningful for this analysis than the absolute energy values themselves.

The total intraprotein electrostatic energy exhibits a slight increase, by 24 kcal/mol for tm_gdh and by 6 kcal/mol for cs_gdh, when the temperature increases to 343 K, followed by large decreases (more negative values) of 170 and by 91 kcal/mol, respectively, when the temperature increases to 373 K. The main contributions to these changes come from the interactions between the positively charged and negatively charged residues (Pos−Neg), on one hand, and charged residues and noncharged residues (Chrg−Nchrg), on the other. For the tm_gdh protein in the simulation at 343 K, less favorable interactions are observed between the charged and noncharged residues (Chrg−Nchrg, $\Delta E_{343-300}$ = 65 kcal/mol), while for the cs_gdh protein, less favorable interactions are observed between the positively charged and negatively charged residues (Pos−Neg, $\Delta E_{343-300}$ = 65 kcal/mol). At 373 K, the Pos−Neg electrostatic interactions for the tm_gdh protein become more favorable by 111 kcal/mol, while for cs_gdh, the Pos−Neg interactions become more favorable by only 34 kcal/mol. It has to be noted that at 373 K all the contributions to the intraprotein electrostatic energy become more favorable than at 300 K in the case of tm_gdh; this indicates an optimized spatial arrangement of all residues at this temperature.

Ion Pairs and Salt Bridges. The distances between the functional groups of the charged residues in the starting structures were calculated by applying a distance cutoff of 9 Å. Within this cutoff, the initial structure of tm_gdh comprises 20 oppositely charged pairs and 19 identically

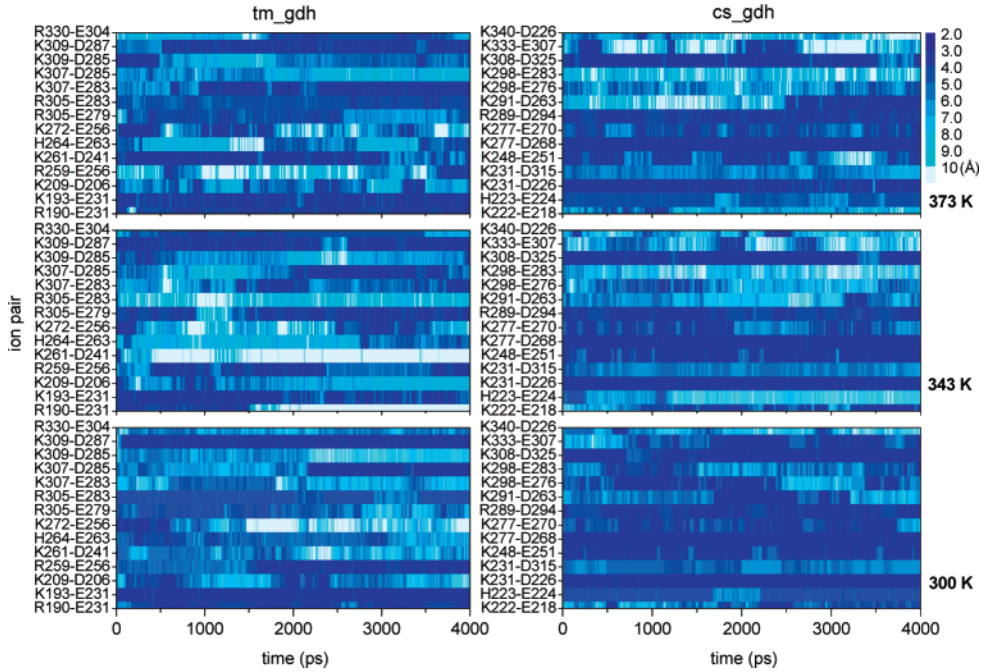

FIGURE 6: Dynamic behavior of the ion pairs of tm_gdh and cs_gdh in the MD simulations at 300, 343, and 373 K. The interaction distance is represented on a scale from 2 to 10 Å.

charged pairs, whereas the initial structure of cs_gdh comprises 28 oppositely charged pairs and 14 identically charged pairs. The larger number of pairs of oppositely charged residues separated by distances shorter than 9 Å suggests a more favorable electrostatic interaction in the cs_gdh protein than in tm_gdh at 300 K, which was confirmed by the calculation of electrostatic energy presented in Table 1 (for tm_gdh, $E_{\mathrm{Pos-Neg}} = -680$ kcal/mol; for cs_gdh, $E_{\mathrm{Pos-Neg}} = -800$ kcal/mol). However, due to the difference in the spatial distribution of the charged residues, small fluctuations of the side chains as well as small conformational changes of the protein backbone are expected to alter the energy contributions differently for tm_gdh versus cs_gdh.

The analysis of the changes in the electrostatic energy terms was complemented by an examination of the dynamic behavior of the charged residues in general and more specifically of the ion pairs located at distances that allow the formation of salt bridges. For this purpose, the distances between the functional groups of all positively charged and all negatively charged residues were calculated as a function of time from the MD trajectories of tm_gdh and cs_gdh at all simulation temperatures. To consider only the ion pairs that are responsible for the main energetic contribution, we applied a distance criterion, and those pairs that were, at some moment, closer than 6 Å were selected. The dynamic behavior of the ion pairs within tm_gdh and cs_gdh at different simulation temperatures is presented in Figure 6.

Although ~17 ion pairs of the tm_gdh protein have formed salt bridges at certain times during the simulations at 300, 343, and 373 K, only ~6 ion pairs remained stable throughout the simulations. Most of the ion pairs connect adjacent loops and adjacent helices. Thus, helices H1 and H2 are connected on the solvent-exposed side by the Arg190-(H1)-Glu231(H2)-Lys193(H1) salt bridge triad which is stable in all simulations except for the simulation at 500 K. Another triad, Glu256-Arg259-Glu263, is located on the external side of H3; the Glu256-Arg259 and Glu263-Arg259 pairs have slightly different stabilities. The Glu263-Arg259 pair remains stable at higher temperatures (343 and 373 K), while Glu256 interacts more strongly with Lys272 located on the loop between H3 and β4. The Asp241-Lys261 pair connects the C-terminus of β2 with H3 and shows a much stronger interaction at 300 and 343 K. The Glu279-Arg305-Glu283 triad which connects helices H1 and H2 exhibits less strength at 343 K, but it becomes stronger at 373 K, with almost equal interacting distances between the Arg305-Glu279 and Arg305-Glu283 pairs. The adjacent H4−β5 and H5−β6 loops are connected by the Lys309-Asp287 salt bridge which is stable at all simulation temperatures.

The cs_gdh protein fragment shows approximately seven salt bridges that are stable throughout the simulation at 300 K, but only five of them remain stable at 343 and 373 K (Figure 6). The His223-Glu224 pair is located on helix H1 and is stable at the simulation temperatures 300 and 373 K. A stronger salt bridge is formed by Asp226 and Lys231 which connect the C-terminus of H1 and the N-terminus of β1. Helix H2 has three charged residues located on its solvent-exposed side; the Lys248-Glu251 pair is stronger and more stable than the Lys247-Glu251 pair throughout all simulations. The long loop between β3 and H3 is anchored to helix H3 by the Asp268-Lys277-Glu270 triad which is stable at all simulation temperatures; a part of this loop is buried in the protein hydrophobic core, and this can explain its low flexibility as compared with those of the other loops. Another strong salt bridge is formed by Arg289 and Asp294 located on the loop between H3 and H4 and on helix H4, respectively. The adjacent β4−β5 and β5−H5 loops are linked by a stable salt bridge, Lys308-Asp325. The C-terminal part of cs_gdh (including helices H5 and H6, strands β6 and β7, and the loops connecting these elements), although comprising four positively charged and four negatively charged residues, does not show any strongly interacting ion pair.

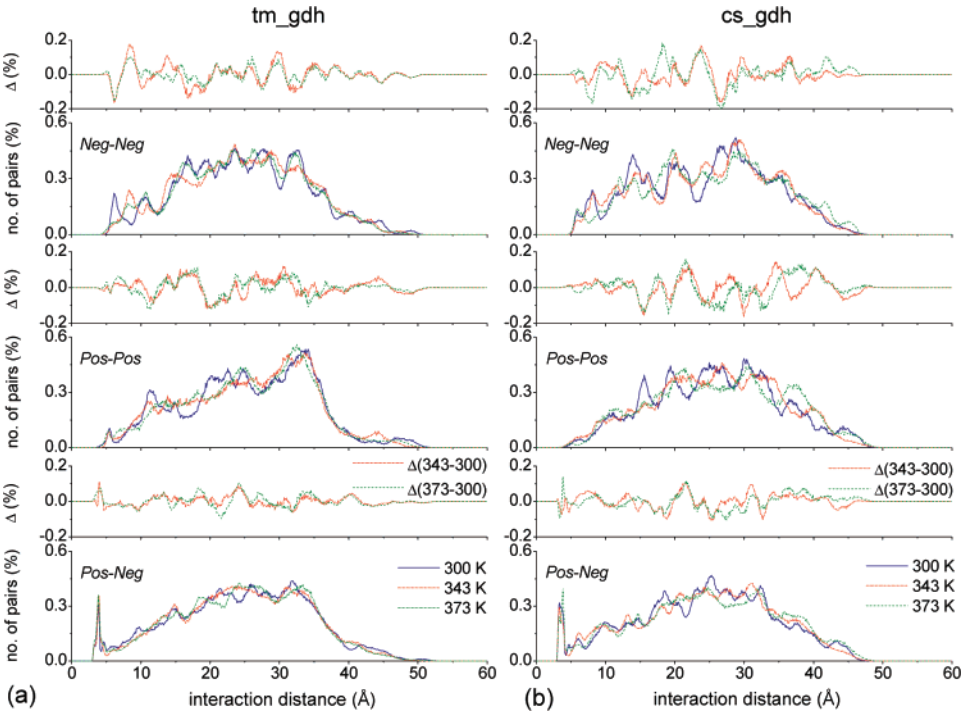

FIGURE 7: Distance distributions of all charged side chains of tm_gdh (a) and cs_gdh (b), calculated from the MD simulations at 300, 343, and 373 K.

Positional Fluctuations of the Charged Residues. The changes in the electrostatic energy contributions of various charged groups with an increase in temperature were explained by considering the positional displacements of the charged side chains as a result of their local fluctuations induced by elevated temperatures. Distance distributions for all pairs of charged residues of both protein fragments were calculated from the simulations at 300, 343, and 373 K and are displayed in Figure 7 (see Materials and Methods). Relative changes in the distance distribution were calculated for the simulation temperatures of 343 and 373 K with respect to the interaction distance distribution at 300 K. Changes in the distance distribution with an increase in temperature are observed for all three types of interacting pairs (positive−negative, positive−positive, and negative−negative).

The electrostatic energies would be mostly affected by the redistribution of the interaction distances located in the distance interval of 2.5−20 Å. Although changes of various magnitudes in the interaction distance distribution are observed for all interacting subgroups, it is not straightforward to estimate, on the basis of these data, if they contribute favorably or unfavorably to the intramolecular electrostatic energies of these protein fragments. However, the evidence of a certain displacement of the charged residues observed in the MD simulations at elevated temperatures suggested to us to quantify the contribution of the ionizable residues to the thermal stability of the protein by taking into account the dynamic arrangement of the charged side chains.

Electrostatic Contributions to the Free Energy of Folding. We have computed the electrostatic free energy contributions of the salt bridge-forming residues to the stability of tm_gdh and cs_gdh fragments using three-dimensional structures obtained from MD simulations of the proteins at 300, 343, and 373 K (as described in Materials and Methods). The thermodynamics of the formation of salt bridges in the folded proteins were analyzed by employing a thermodynamic cycle defined previously in the literature (*11*). Thus, the electrostatic contribution of each salt bridge to protein stability was decomposed into three terms that account for the solvation process during folding ($\Delta\Delta G_{desolv}$), the interaction between the two side chains in the folded protein ($\Delta\Delta G_{bridge}$), and the interaction of the ion pair with the other residues in the protein ($\Delta\Delta G_{prt}$). Each term was computed using continuum electrostatics. For these calculations, we selected the ion pairs that exhibited the shortest interaction distances throughout the simulations (i.e., longer time in the salt bridge length range). One set of ion pairs (tm_gdh) comprises 11 positively and 10 negatively charged residues, whereas the other set of ion pairs (cs_gdh) comprises 11 positively and 13 negatively charged residues. The two sets involve a similar number of charged residues and therefore allow a proper comparison of the energetic contribution of salt bridges to the stability of tm_gdh and cs_gdh.

The free energy terms calculated from MD trajectories at 300, 343, and 373 K are presented in Tables 2 (tm_gdh) and 3 (cs_gdh). The electrostatic free energies of the ion pairs ($\Delta\Delta G_{tot}$) have negative values for both protein fragments at all three simulation temperatures. For tm_gdh, the average values of $\Delta\Delta G_{tot}$ decrease at elevated temperatures, namely, by ∼1 kcal/mol at 343 K and 1.7 kcal/mol at 373K, relative to the calculation at 300 K. For cs_gdh, the mean value of $\Delta\Delta G_{tot}$ at 343 K does not change compared to the mean $\Delta\Delta G_{tot}$ at 300 K, but it decreases by 0.7 kcal/mol at 373 K. The electrostatic free energy contribution of the ion pairs calculated at 300 K is, on average, similar for the hyper- and mesophilic protein fragments, lying around −5 kcal/mol. However, the individual contributions of the ion pairs are different for tm_gdh and cs_gdh, as indicated by the standard deviations which differ by ∼1 kcal/mol (±2.40 kcal/mol for tm_gdh as compared with ±3.55 kcal/mol for cs_gdh). The individual $\Delta\Delta G_{tot}$ values are closer to

Table 2: Electrostatic Free Energy Contributions for tm_gdh Computed from Series of MD Snapshots at 300, 343, and 373 K[a]

salt bridge	$\Delta\Delta G_{dslv}$ (kcal/mol)	$\Delta\Delta G_{brd}$ (kcal/mol)	$\Delta\Delta G_{prt}$ (kcal/mol)	$\Delta\Delta G_{tot}$ (kcal/mol)
		300 K ($\epsilon_w = 80$)		
R190−E231	8.20 (1.04)	−9.38 (2.63)	−6.29 (1.12)	−7.47 (1.59)
K193−E231	8.90 (1.02)	−7.80 (1.09)	−8.38 (2.35)	−7.28 (1.73)
K209−D206	6.68 (2.06)	−2.15 (2.45)	−9.58 (4.43)	−5.05 (3.28)
R259−E256	5.86 (1.19)	−5.80 (3.71)	−8.07 (3.40)	−8.02 (3.15)
K261−D241	10.82 (3.80)	−1.86 (1.85)	−12.10 (4.70)	−3.14 (2.60)
H264−E263	2.79 (0.74)	−1.04 (0.86)	−2.05 (1.81)	−0.30 (1.20)
K272−E256	4.59 (1.26)	−1.74 (2.53)	−8.05 (2.81)	−5.20 (1.67)
R305−E279	3.40 (1.15)	−2.80 (1.92)	−7.12 (1.75)	−6.52 (1.93)
R305−E283	7.45 (1.42)	−6.87 (1.65)	−2.59 (2.33)	−2.00 (2.10)
K307−E283	8.07 (2.00)	−1.38 (1.15)	−12.54 (3.08)	−5.84 (2.47)
K307−D285	5.59 (1.76)	−3.84 (3.14)	−4.86 (3.14)	−3.11 (1.76)
K309−D285	5.22 (1.15)	−1.04 (0.39)	−10.46 (3.59)	−6.28 (2.52)
K309−D287	9.30 (1.53)	−8.01 (1.55)	−7.28 (1.38)	−5.98 (1.30)
R330−E304	2.60 (0.85)	−0.89 (0.17)	−3.37 (1.72)	−1.67 (1.12)
average	6.39 (2.53)	−3.90 (3.03)	−7.34 (3.28)	−4.85 (2.40)
		343 K ($\epsilon_w = 62$)		
R190−E231	6.63 (2.91)	−4.37 (5.12)	−10.55 (8.15)	−8.29 (5.30)
K193−E231	6.18 (3.39)	−6.38 (2.93)	−3.88 (4.28)	−4.07 (3.03)
K209−D206	5.44 (2.75)	−1.25 (1.05)	−8.69 (5.64)	−4.50 (2.84)
R259−E256	6.84 (1.45)	−5.98 (4.19)	−9.75 (5.96)	−8.89 (3.42)
K261−D241	11.18 (3.40)	−1.08 (1.63)	−17.81 (7.02)	−7.70 (4.04)
H264−E263	3.29 (1.07)	−1.31 (1.06)	−3.50 (2.96)	−1.52 (2.05)
K272−E256	5.72 (1.83)	−3.35 (3.62)	−9.02 (5.15)	−6.65 (2.84)
R305−E279	6.31 (1.74)	−8.11 (3.47)	−2.63 (1.67)	−4.43 (2.10)
R305−E283	3.92 (1.26)	−0.94 (0.73)	−9.28 (4.22)	−6.29 (3.56)
K307−E283	3.80 (1.40)	−2.30 (1.91)	−6.87 (4.22)	−5.36 (3.44)
K307−D285	5.17 (1.73)	−3.97 (3.32)	−5.93 (2.64)	−4.73 (2.73)
K309−D285	5.82 (1.50)	−1.58 (1.39)	−10.57 (3.11)	−6.33 (2.19)
K309−D287	9.99 (1.78)	−8.34 (2.21)	−8.24 (2.24)	−6.59 (2.19)
R330−E304	7.34 (2.96)	−6.96 (3.53)	−6.58 (5.14)	−6.19 (3.59)
average	6.26 (2.19)	−3.99 (2.72)	−8.09 (3.81)	−5.82 (1.91)
		373 K ($\epsilon_w = 56$)		
R190−E231	8.00 (1.30)	−10.01 (2.22)	−5.50 (2.15)	−7.51 (2.09)
K193−E231	8.63 (1.52)	−7.54 (2.53)	−8.38 (2.14)	−7.29 (1.84)
K209−D206	5.97 (2.60)	−2.71 (2.71)	−8.50 (4.90)	−5.23 (3.41)
R259−E256	5.10 (1.53)	−1.64 (2.29)	−10.74 (5.69)	−7.29 (4.06)
K261−D241	11.95 (2.87)	−8.63 (4.01)	−8.57 (2.60)	−5.25 (1.77)
H264−E263	4.38 (1.47)	−1.37 (0.77)	−6.13 (3.05)	−3.12 (1.97)
K272−E256	4.99 (2.22)	−4.21 (3.81)	−5.69 (2.89)	−4.90 (2.88)
R305−E279	4.78 (1.56)	−3.85 (2.61)	−9.79 (4.03)	−8.86 (2.86)
R305−E283	8.07 (1.76)	−7.08 (1.52)	−9.87 (4.45)	−8.88 (3.85)
K307−E283	8.73 (2.58)	−7.05 (3.67)	−9.84 (2.85)	−8.16 (2.99)
K307−D285	6.18 (1.53)	−1.59 (1.40)	−11.83 (4.19)	−7.24 (3.12)
K309−D285	6.13 (1.97)	−3.09 (2.85)	−8.67 (2.29)	−5.63 (1.88)
K309−D287	10.38 (1.70)	−8.07 (2.72)	−10.10 (4.27)	−7.79 (2.54)
R330−E304	5.37 (1.44)	−4.86 (3.86)	−4.15 (2.91)	−3.64 (1.41)
average	7.05 (2.29)	−5.12 (2.90)	−8.41 (2.24)	−6.49 (1.85)

[a] Standard deviations are given in parentheses.

Table 3: Electrostatic Free Energy Contributions for cs_gdh Computed from Series of MD Snapshots at 300, 343, and 373 K[a]

salt bridge	$\Delta\Delta G_{dslv}$ (kcal/mol)	$\Delta\Delta G_{brd}$ (kcal/mol)	$\Delta\Delta G_{prt}$ (kcal/mol)	$\Delta\Delta G_{tot}$ (kcal/mol)
		300 K ($\epsilon_w = 80$)		
K222−E218	2.63 (1.49)	−2.38 (2.14)	−1.63 (0.23)	−1.37 (1.09)
H223−E224	3.74 (0.62)	−5.03 (1.25)	−0.40 (0.27)	−1.69 (0.95)
K231−D226	10.46 (1.58)	−9.35 (1.55)	−7.63 (2.07)	−6.52 (1.78)
K231−D315	8.25 (1.19)	−1.69 (0.27)	−16.98 (2.94)	−10.42 (1.96)
K248−E251	4.76 (1.10)	−6.14 (1.88)	−1.30 (0.97)	−2.68 (1.36)
K277−D268	20.58 (1.97)	−14.97 (2.18)	−15.15 (3.10)	−9.54 (2.64)
K277−E270	9.24 (1.61)	−5.04 (3.05)	−15.28 (1.95)	−11.08 (2.18)
R289−D294	11.08 (1.59)	−11.10 (1.26)	−2.85 (0.89)	−2.86 (1.20)
K291−D263	11.31 (4.50)	−4.28 (4.04)	−11.19 (5.53)	−4.16 (2.52)
K298−E276	5.13 (1.95)	−3.63 (2.93)	−4.27 (2.93)	−2.77 (2.47)
K298−E283	5.21 (2.93)	−2.85 (3.16)	−4.28 (2.59)	−1.91 (2.50)
K308−D325	10.26 (1.41)	−8.94 (1.54)	−4.84 (2.02)	−3.51 (1.77)
K333−E307	6.37 (2.44)	−4.36 (2.96)	−4.54 (2.18)	−2.53 (1.79)
K340−D226	7.99 (1.66)	−1.62 (1.62)	−15.48 (2.81)	−9.10 (2.15)
average	8.36 (4.52)	−5.81 (3.92)	−7.56 (6.00)	−5.01 (3.55)
		343 K ($\epsilon_w = 62$)		
K222−E218	4.27 (1.92)	−3.83 (2.80)	−1.72 (0.65)	−1.28 (1.40)
H223−E224	2.51 (0.82)	−1.46 (1.26)	−1.04 (1.27)	0.02 (1.40)
K231−D226	10.78 (1.97)	−9.94 (1.57)	−7.99 (3.21)	−7.15 (2.39)
K231−D315	9.14 (1.19)	−1.93 (0.25)	−17.32 (3.10)	−10.11 (2.46)
K248−E251	5.68 (1.38)	−6.51 (2.34)	−2.29 (1.83)	−3.11 (1.75)
K277−D268	20.00 (1.69)	−14.96 (2.34)	−13.81 (3.18)	−8.77 (2.49)
K277−E270	8.63 (1.47)	−4.40 (3.16)	−15.47 (3.24)	−11.25 (2.02)
R289−D294	11.88 (2.22)	−10.62 (2.29)	−4.91 (3.98)	−3.65 (2.46)
K291−D263	11.95 (5.40)	−1.81 (1.07)	−15.12 (8.66)	−4.98 (4.06)
K298−E276	2.20 (1.30)	−1.88 (1.68)	−2.46 (0.98)	−2.14 (0.91)
K298−E283	2.25 (1.09)	−0.90 (0.33)	−4.06 (2.22)	−2.70 (1.63)
K308−D325	10.27 (2.29)	−9.48 (1.98)	−4.55 (2.14)	−3.77 (1.70)
K333−E307	3.60 (2.18)	−1.74 (1.82)	−3.50 (1.59)	−1.64 (0.78)
K340−D226	8.19 (1.93)	−2.22 (2.38)	−15.78 (3.66)	−9.82 (2.60)
average	7.95 (5.00)	−5.12 (4.44)	−7.86 (6.18)	−5.03 (3.70)
		373 K ($\epsilon_w = 56$)		
K222−E218	4.11 (1.61)	−2.12 (2.47)	−5.55 (3.15)	−3.56 (2.09)
H223−E224	3.29 (0.92)	−4.84 (1.84)	−0.68 (1.33)	−2.23 (1.60)
K231−D226	9.17 (2.31)	−8.77 (2.23)	−6.24 (3.00)	−5.85 (2.44)
K231−D315	8.92 (1.65)	−2.08 (0.99)	−17.57 (4.71)	−10.73 (3.28)
K248−E251	5.20 (1.36)	−4.64 (3.11)	−5.89 (3.08)	−5.32 (2.51)
K277−D268	21.14 (2.05)	−16.89 (2.05)	−14.53 (3.17)	−10.28 (2.62)
K277−E270	9.12 (1.69)	−4.75 (3.02)	−15.44 (2.25)	−11.08 (2.03)
R289−D294	10.97 (2.92)	−11.30 (1.87)	−6.47 (5.01)	−6.81 (3.60)
K291−D263	7.65 (3.19)	−4.50 (4.46)	−8.07 (6.15)	−4.91 (2.68)
K298−E276	2.20 (1.27)	−2.06 (1.99)	−2.15 (0.76)	−2.01 (1.30)
K298−E283	2.30 (1.14)	−0.90 (0.32)	−4.14 (2.31)	−2.75 (1.74)
K308−D325	10.82 (3.32)	−9.45 (3.25)	−4.99 (2.39)	−3.63 (2.33)
K333−E307	3.53 (2.37)	−2.45 (2.98)	−3.20 (2.18)	−2.11 (2.00)
K340−D226	6.79 (2.30)	−1.91 (2.43)	−13.35 (4.14)	−8.47 (2.91)
average	7.52 (4.98)	−5.48 (4.56)	−7.73 (5.32)	−5.70 (3.29)

[a] Standard deviations are given in parentheses.

the mean value for tm_gdh, whereas they are more dispersed for cs_gdh. Four ion pairs within cs_gdh (K231 and D315, K277 and D268, K277 and E270, and K340 and D226) make large favorable free energy contributions ranging from −9 to −11 kcal/mol, while the other ion pairs make contributions significantly smaller than the mean value. The same trend of the individual $\Delta\Delta G_{tot}$ values is encountered for both protein domains at higher temperatures. Unlike the ion pairs of cs_gdh which do not undergo changes in the magnitudes of their energetic contributions with an increase in temperature, the ion pairs of tm_gdh exhibit larger favorable contributions (i.e., more negative $\Delta\Delta G_{tot}$) and less dispersed $\Delta\Delta G_{tot}$ values as indicated by their lower standard deviations [±1.91 kcal/mol at 343 K and ±1.85 kcal/mol at 373 K (Table 2)].

The formation of a salt bridge is favorable for the folded protein if the desolvation energy penalty ($\Delta\Delta G_{dslv}$) is surpassed in magnitude by the favorable contributions due to the interaction of the salt-bridging residues with each other ($\Delta\Delta G_{brd}$) and with the neighboring residues ($\Delta\Delta G_{prt}$). For only a few ion pairs belonging to either tm_gdh or cs_gdh is the desolvation penalty compensated by and slightly exceeded by the salt bridge energy term $\Delta\Delta G_{brd}$ alone (Tables 2 and 3). The average $\Delta\Delta G_{brd}$ values at all simulation temperatures are smaller (as absolute values) by ~2.5 kcal/mol than the mean values of the desolvation term ($\Delta\Delta G_{dslv}$). On the other hand, for both protein fragments, the protein interaction term ($\Delta\Delta G_{prt}$) makes a substantial favorable contribution (average of approximately −7.5 kcal/mol) to the total free energy change ($\Delta\Delta G_{tot}$). However, in the cs_gdh fragment, the protein environment strongly stabilizes only five ion pairs ($\Delta\Delta G_{prt}$ from −11 to −17 kcal/mol), while in tm_gdh, the surrounding protein has a more uniform contribution stabilizing substantially most of the ion pairs

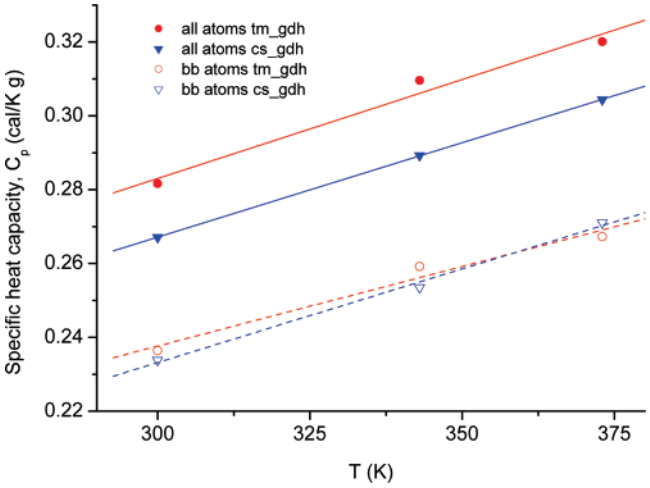

FIGURE 8: Specific heat capacities of tm_gdh and cs_gdh calculated for the whole protein and for the protein backbone alone from the MD trajectories at 300, 343, and 373 K.

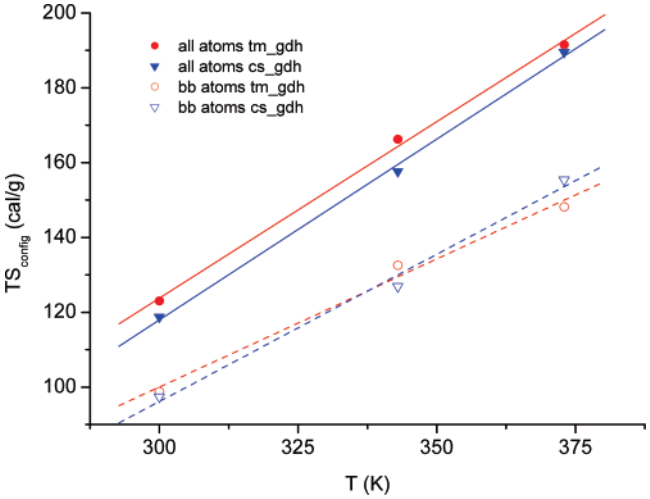

FIGURE 9: Configurational entropies of tm_gdh and cs_gdh calculated for the whole protein and for the protein backbone alone from the MD trajectories at 300, 343, and 373 K.

(Tables 2 and 3). Furthermore, for tm_gdh, the average $\Delta\Delta G_{prt}$ decreases with an increase in temperature (it becomes −8.4 kcal/mol at 373 K), whereas for cs_gdh, it changes insignificantly at elevated temperatures.

Heat Capacities and Entropies. The heat capacity of proteins in aqueous solution arises from a major contribution of the protein itself due to its intrinsic covalent and noncovalent interactions and a smaller contribution due to the interaction of the protein with the solvent, so it can be written as

$$C_p = C_p^{\text{bonded}} + C_p^{\text{nonbonded}} + C_p^{\text{hydration}}$$

Our calculation of heat capacity provides an estimation of the intrinsic heat capacity of the protein (the first two terms of the above equation), and due to its underlying contributions, we would call it configurational heat capacity

$$C_p^{\text{config}} = C_p^{\text{bonded}} + C_p^{\text{nonbonded}}$$

According to this definition, the calculated C_p^{config} can be compared to the experimentally determined heat capacity of a native folded protein in the anhydrous state.

The heat capacities calculated for tm_gdh and cs_gdh in the folded state and their dependencies on temperature are presented in Figure 8. The calculations were performed for the whole protein domain, as well as for the protein backbone to assess the contribution to the difference in heat capacity observed between the hyperthermophilic and mesophilic domains. The values of the configurational heat capacities calculated for tm_gdh and cs_gdh from the MD simulations at 300 K are 0.281 and 0.267 cal K^{-1} g^{-1}, respectively, and compare well with the value of 0.298 cal K^{-1} g^{-1} representing an average of experimental heat capacities of various anhydrous proteins (*39*). As observed in Figure 8, there are no significant differences between the heat capacities of tm_gdh and cs_gdh calculated for the protein backbones only.

The configurational entropies of tm_gdh and cs_gdh at different temperatures calculated also for the whole protein domain and for the protein backbone alone are presented in Figure 9. It can be noted that the tm_gdh domain exhibits slightly higher values of the entropy than the cs_gdh domain.

DISCUSSION

The dynamics of a hyperthermophilic protein domain in a water environment was studied by MD simulations at various temperatures and was compared to the dynamical behavior of a homologous mesophilic protein simulated under identical conditions. The role played by the charged residues in the conformational stability of these protein fragments was evaluated by calculating the electrostatic strength of several ion pairs from each protein. The electrostatic free energy terms derived from a thermodynamic cycle were obtained by solving the linearized Poisson−Boltzmann equation for a series of protein conformations generated by MD simulations and placed subsequently in a continuum solvent medium. The motional freedom of the proteins in solution which implies a variety of atomic fluctuations plays an important role in protein stability, and it is taken into consideration in our calculations.

The MD trajectories, each covering a simulation time of 4 ns, showed the conformational stability of both tm_gdh and cs_gdh at 300, 343, and 373 K. Experimental data (*21*) indicate that tm_gdh is stable at 343 K, whereas the mesophilic GluDH domain starts to denature at a lower temperature. Considering the length of our simulations relative to the much larger time scale of the protein unfolding process, the results of the MD simulations are not in contradiction with the experimental observations. The MD trajectory of cs_gdh at 373 K already shows a slight destabilization of the native conformation which is indicated by a higher rms deviation of the backbone atoms (Figure 3) and a general increase in the atomic fluctuations involving all secondary structure elements (Figure 5b). At 500 K, the unfolding of the cs_gdh fragment is evident while tm_gdh still shows thermal tolerance. Protein denaturation has been observed at elevated simulation temperatures in several MD studies (*40*−*43*); however, the high stability of a hyperthermophilic protein simulated at 550 K has also been reported (*15*). Although various factors related to the simulation method itself can artificially stabilize the protein structure (*15*), it is certainly possible that the unexpected thermal

stability is a consequence of the enhanced kinetic stability of hyperthermophilic proteins.

The energetic analysis for tm_gdh and cs_gdh fragments from MD simulations at 300, 343, and 373 K indicated a gain in the electrostatic interaction energy with an increase in temperature for some of the interacting groups (Table 1). A similar observation has been presented by de Bakker et al. (*15*), who attributed the favorable change in the intraprotein electrostatic energy to the tightening of salt bridges. Our data too indicate that the major stabilizing electrostatic energy with increasing temperature comes from the interaction between the oppositely charged interacting groups (Pos−Neg). The ion pairs of the tm_gdh fragment (Figure 6) show a slight shortening of the interaction distances during the simulation at 373 K. Moreover, for tm_gdh, the interactions between the positively charged residues (Pos−Pos) as well as the interactions between the negatively charged residues (Neg−Neg) contribute favorably, although modestly, to the intraprotein electrostatic energy at elevated temperatures. The same favorable trend in the electrostatic contributions is however not observed for the cs_gdh domain. The complementary analysis of the interaction distance distribution of all charged side chains as a function of simulation temperature gives further indications about the atomic positional displacements responsible for the energetic changes within the simulated proteins.

The computed electrostatic free energy contributions of the salt bridge-forming residues to the stability of tm_gdh and cs_gdh using "fluctuating" structures taken from the MD simulations at different temperatures show that the ion pairs are electrostatically stabilizing in all cases but the individual contributions vary significantly. The values of the free energy components $\Delta\Delta G_{dslv}$, $\Delta\Delta G_{brd}$, and $\Delta\Delta G_{prt}$ as well as the values of overall free energy change $\Delta\Delta G_{tot}$ calculated for various ion pairs of tm_gdh and cs_gdh are on the same order of magnitude with data presented for different proteins in a number of theoretical studies (*16*, *18*, *44*).

The results of our study show the positive role played by the spatial placement and mobility of the charged residues within the protein structure in the enhanced thermal stability of a hyperthermophilic protein as compared with its mesophilic homologue. An increased number of ionizable amino acids and their optimum location within the structure have previously been proposed as factors of enhanced stability for hyperthermophilic proteins (*1*, *2*, *7*). The effect of the protein conformational flexibility on the strength of ion pairs has been taken into consideration by Kumar and Nussinov (*18*). They have included NMR conformational ensembles in the continuum electrostatic calculations and found that the contribution of ion pairs varies considerably among the conformers of each protein. In our approach, we assumed that the series of conformations generated by the MD simulations at 300, 343, and 373 K represent more adequately the structure of the proteins in solution, especially at elevated temperatures. The greater contribution of the charged residues to the stability of the hyperthermophilic protein (tm_gdh) as compared with the mesophilic counterpart (cs_gdh) was revealed only by the calculations that included conformations sampled at 343 and 373 K. The hydration of the charged residues decreases with an increase in temperature, and therefore, the magnitude of the desolvation penalty for formation of a salt bridge is diminished at higher temperatures (*14*). As a consequence, at high temperatures, the desolvation penalty is in general outweighed by favorable interactions within the salt bridge and with the neighboring residues, and thus, the salt bridges actually promote protein stability. To separate the computed contribution of the conformers generated at elevated temperatures from the hydration effects at high temperatures, we performed calculations using structures taken from the MD simulations at 300 K but with the dielectric constant of water corresponding to 373 K ($\epsilon_w = 56$). For tm_gdh, the average value of free energy change $\Delta\Delta G_{tot}$ was −5.54 kcal/mol which is ∼1 kcal/mol higher than the average $\Delta\Delta G_{tot}$ calculated for the conformers generated at 373 K (Table 2) and ∼0.70 kcal/mol lower than the free energy change calculated for the conformers generated at 300 K (and using an ϵ_w of 80). This result indicates that a significant favorable contribution to the free energy change comes from the conformational variability rather than from the hydration effects and a large decrease in the dielectric constant of water. In contrast, for the mesophilic cs_gdh fragment, the free energy change (average $\Delta\Delta G_{tot} = -5.72$ kcal/mol, for conformers at 300 K but with an ϵ_w of 56) is ∼0.70 kcal/mol smaller than the free energy change calculated for the conformers generated at 300 K and using an ϵ_w of 80 (Table 3), but it is on the same order of magnitude with the mean value calculated for the conformers generated at 373 K. These data suggest that the conformational variability of the cs_gdh fragment simulated at elevated temperatures does not make a favorable contribution to the electrostatic free energy change.

Our results regarding the role played by the distribution of charges in the protein structure as well as their mobility are consistent with a recent study by Dominy et al. (*45*) that indicated as key factors in thermostability the electrostatic interactions of charged residues in the folded state and the dielectric response of the folded protein. The dielectric response is closely related to the number and distribution of charges present within a protein, and the calculated values of the dielectric response were found to increase with the experimentally observed thermal stability. The authors calculated the dielectric response of the protein on the basis of the atomic fluctuations sampled from a MD simulation, and the result suggests that the effect of dynamics on the charge distribution varies with thermostability, as clearly observed in our study.

Measurements of the heat capacity changes, ΔC_p, upon thermal denaturation of proteins show lower changes in heat capacity for most of the hyperthermophilic proteins as compared with (homologous) mesophilic proteins (*46*); i.e., $\Delta C_p^{\text{unfoldingthermophile}} < \Delta C_p^{\text{unfoldingmesophile}}$. The heat capacity change, ΔC_p, represents the difference between absolute heat capacities of the unfolded and folded states ($\Delta C_p = C_p^{\text{unfolded}} - C_p^{\text{folded}}$).

The difference between the heat capacity of the native and denatured state originates from changes in two of the heat capacity components, namely, $C_p^{\text{nonbonded}}$ and $C_p^{\text{hydration}}$, as a result of the loss of native noncovalent interactions (which define the secondary and tertiary structure) and an increased number of polar and nonpolar residues exposed to solvent upon unfolding.

Thus, previous studies attributed the smaller heat capacity change in thermophilic proteins to the solvent interactions

with the folded and unfolded state (which correlates with the changes in the solvent-accessible surface areas) (*47*, *48*) and to some residual structure found in the unfolded state of a thermophilic protein (*46*). Our calculations show that the specific heat capacity of the hyperthermophilic tm_gdh domain in the folded state is higher than the specific heat capacity of the mesophilic cs_gdh (Figure 1). Although it cannot yet be generalized to other proteins since we calculated heat capacities only for these two homologous protein domains, this finding may have important implications for the mechanism of stabilization of hyperthermophilic proteins. A higher value of C_p^{config} for the native state implies a decrease in the ΔC_p between the unfolded and folded state, thus representing another factor that contributes to the large difference in ΔC_p observed between hyperthermophilic and mesophilic proteins. The heat capacity change upon unfolding determines the curvature ($\partial^2 \Delta G/\partial T^2 = -\Delta C_p/T$) of the protein stability curve [$\Delta G_U = f(T)$], so a reduction of the ΔC_p would result in a flatter curve and consequently a higher denaturation temperature (T_m).

Since heat capacity is a measure of the mean fluctuation in energy, both the fluctuations of the protein between different states and the energy changes with the transition between states play an important role in determining the value of C_p. Taking into consideration the results of the configurational entropy calculations, we can interpret the slightly higher entropy of the tm_gdh domain (Figure 9) as an indication of a higher degeneracy of the accessible energy states as compared with the energy states accessible to the cs_gdh domain. The degeneracy of the higher energy levels is a consequence of the nonbonded interactions available to a protein during its dynamics. We speculate that the distribution of the charged residues within the structure of the tm_gdh domain (as electrostatic interactions are long-range) may determine a degeneracy of the energy states. This is consistent with our results presented in Tables 2 and 3, where the $\Delta\Delta G_{\text{prt}}$ term representing the electrostatic free energy due to the interaction of the selected ion pairs with the rest of the protein (i.e., it accounts for a network of interactions) shows values distributed over a smaller range for tm_gdh (standard deviation of ~3 kcal/mol) as compared with that for the cs_gdh domain (standard deviation of ~6 kcal/mol).

In our attempt to determine the contributions to the stability of a hyperthermophilic protein, we considered the solvated protein in its dynamic context, and we calculated thermodynamic properties such as electrostatic free energy differences on one hand and configurational entropy and heat capacity on the other hand which provided new insight into the mechanism of protein thermostabilization. The dynamical behavior of the two proteins studied in this work and the thermodynamic calculations suggest that the hyperthermophilic protein possesses an optimized placement of the charged residues within its structure that allows them to interact more cooperatively and thus more favorably during the conformational fluctuations of the protein in the aqueous environment.

REFERENCES

1. Karshikoff, A., and Ladenstein, R. (2001) Ion pairs and the thermotolerance of proteins from hyperthermophiles: A 'traffic rule' for hot roads, *Trends Biochem. Sci. 26*, 550−556.
2. Spassov, V. Z., Karshikoff, A. D., and Ladenstein, R. (1994) Optimization of the Electrostatic Interactions in Proteins of Different Functional and Folding Type, *Protein Sci. 3*, 1556−1569.
3. Yip, K. S. P., Stillman, T. J., Britton, K. L., Artymiuk, P. J., Baker, P. J., Sedelnikova, S. E., Engel, P. C., Pasquo, A., Chiaraluce, R., Consalvi, V., Scandurra, R., and Rice, D. W. (1995) The Structure of *Pyrococcus furiosus* Glutamate Dehydrogenase Reveals a Key Role for Ion-Pair Networks in Maintaining Enzyme Stability at Extreme Temperatures, *Structure 3*, 1147−1158.
4. Kumar, S., and Nussinov, R. (2001) How do thermophilic proteins deal with heat? *Cell. Mol. Life Sci. 58*, 1216−1233.
5. Vogt, G., and Argos, P. (1997) Protein thermal stability: Hydrogen bonds or internal packing? *Folding Des. 2*, S40−S46.
6. Vogt, G., Woell, S., and Argos, P. (1997) Protein thermal stability, hydrogen bonds, and ion pairs, *J. Mol. Biol. 269*, 631−643.
7. Xiao, L., and Honig, B. (1999) Electrostatic contributions to the stability of hyperthermophilic proteins, *J. Mol. Biol. 289*, 1435−1444.
8. Perutz, M. F., and Raidt, H. (1975) Stereochemical Basis of Heat-Stability in Bacterial Ferredoxins and in Hemoglobin-A2, *Nature 255*, 256−259.
9. Perutz, M. F. (1978) Electrostatic Effects in Proteins, *Science 201*, 1187−1191.
10. Dominy, B. N., Perl, D., Schmid, F. X., and Brooks, C. L. (2002) The effects of ionic strength on protein stability: The cold shock protein family, *J. Mol. Biol. 319*, 541−554.
11. Hendsch, Z. S., and Tidor, B. (1994) Do Salt Bridges Stabilize Proteins: A Continuum Electrostatic Analysis, *Protein Sci. 3*, 211−226.
12. Waldburger, C. D., Schildbach, J. F., and Sauer, R. T. (1995) Are Buried Salt Bridges Important for Protein Stability and Conformational Specificity, *Nat. Struct. Biol. 2*, 122−128.
13. Hendsch, Z. S., Jonsson, T., Sauer, R. T., and Tidor, B. (1996) Protein stabilization by removal of unsatisfied polar groups: Computational approaches and experimental tests, *Biochemistry 35*, 7621−7625.
14. Elcock, A. H. (1998) The stability of salt bridges at high temperatures: Implications for hyperthermophilic proteins, *J. Mol. Biol. 284*, 489−502.
15. de Bakker, P. I. W., Hunenberger, P. H., and McCammon, J. A. (1999) Molecular dynamics simulations of the hyperthermophilic protein Sac7d from *Sulfolobus acidocaldarius*: Contribution of salt bridges to thermostability, *J. Mol. Biol. 285*, 1811−1830.
16. Kumar, S., Ma, B. Y., Tsai, C. J., and Nussinov, R. (2000) Electrostatic strengths of salt bridges in thermophilic and mesophilic glutamate dehydrogenase monomers, *Proteins 38*, 368−383.
17. Kumar, S., and Nussinov, R. (2000) Fluctuations between stabilizing and destabilizing electrostatic contributions of ion pairs in conformers of the c-Myc-Max leucine zipper, *Proteins 41*, 485−497.
18. Kumar, S., and Nussinov, R. (2001) Fluctuations in ion pairs and their stabilities in proteins, *Proteins 43*, 433−454.
19. Thomas, A. S., and Elcock, A. H. (2004) Molecular simulations suggest protein salt bridges are uniquely suited to life at high temperatures, *J. Am. Chem. Soc. 126*, 2208−2214.
20. Knapp, S., deVos, W. M., Rice, D., and Ladenstein, R. (1997) Crystal structure of glutamate dehydrogenase from the hyperthermophilic eubacterium *Thermotoga maritima* at 3.0 angstrom resolution, *J. Mol. Biol. 267*, 916−932.
21. Lebbink, J. H. G., Consalvi, V., Chiaraluce, R., Berndt, K. D., and Ladenstein, R. (2002) Structural and thermodynamic studies on a salt-bridge triad in the NADP-binding domain of glutamate dehydrogenase from *Thermotoga maritima*: Cooperativity and electrostatic contribution to stability, *Biochemistry 41*, 15524−15535.
22. Eargle, J., Wright, D., and Luthey-Schulten, Z. (2006) Multiple alignment of protein structures and sequences for VMD, *Bioinformatics 22*, 504−506.
23. Brooks, B. R., Bruccoleri, R. E., Olafson, B. D., States, D. J., Swaminathan, S., and Karplus, M. (1983) Charmm: A Program for Macromolecular Energy, Minimization, and Dynamics Calculations, *J. Comput. Chem. 4*, 187−217.
24. MacKerell, A. D., Bashford, D., Bellott, M., Dunbrack, R. L., Evanseck, J. D., Field, M. J., Fischer, S., Gao, J., Guo, H., Ha, S., Joseph-McCarthy, D., Kuchnir, L., Kuczera, K., Lau, F. T. K., Mattos, C., Michnick, S., Ngo, T., Nguyen, D. T., Prodhom,

B., Reiher, W. E., Roux, B., Schlenkrich, M., Smith, J. C., Stote, R., Straub, J., Watanabe, M., Wiorkiewicz-Kuczera, J., Yin, D., and Karplus, M. (1998) All-atom empirical potential for molecular modeling and dynamics studies of proteins, *J. Phys. Chem. B 102*, 3586−3616.

25. Jorgensen, W. L., Chandrasekhar, J., Madura, J. D., Impey, R. W., and Klein, M. L. (1983) Comparison of Simple Potential Functions for Simulating Liquid Water, *J. Chem. Phys. 79*, 926−935.
26. Andersen, H. C. (1980) Molecular-Dynamics Simulations at Constant Pressure and/or Temperature, *J. Chem. Phys. 72*, 2384−2393.
27. Nose, S., and Klein, M. L. (1983) Constant Pressure Molecular Dynamics for Molecular Systems, *Mol. Phys. 50*, 1055−1076.
28. Hoover, W. G. (1985) Canonical Dynamics Equilibrium Phase-Space Distributions, *Phys. Rev. A 31*, 1695−1697.
29. Ryckaert, J. P., Ciccotti, G., and Berendsen, H. J. C. (1977) Numerical Integration of Cartesian Equations of Motion of a System with Constraints: Molecular Dynamics of N-Alkanes, *J. Comput. Phys. 23*, 327−341.
30. Norberg, J., and Nilsson, L. (2000) On the truncation of long-range electrostatic interactions in DNA, *Biophys. J. 79*, 1537−1553.
31. Frishman, D., and Argos, P. (1995) Knowledge-based protein secondary structure assignment, *Proteins 23*, 566−579.
32. Nina, M., Beglov, D., and Roux, B. (1997) Atomic radii for continuum electrostatics calculations based on molecular dynamics free energy simulations, *J. Phys. Chem. B 101*, 5239−5248.
33. Im, W., Beglov, D., and Roux, B. (1998) Continuum Solvation Model: Computation of electrostatic forces from numerical solutions to the Poisson-Boltzmann equation, *Comput. Phys. Commun. 111*, 59−75.
34. Richards, F. M. (1977) Areas, Volumes, Packing, and Protein-Structure, *Annu. Rev. Biophys. Bioeng. 6*, 151−176.
35. Owen, B. B., Milner, C. E., Miller, R. C., and Cogan, H. L. (1961) Dielectric Constant of Water as a Function of Temperature and Pressure, *J. Phys. Chem. 65*, 2065−2070.
36. Akerlof, G. C., and Oshry, H. I. (1950) The Dielectric Constant of Water at High Temperatures and in Equilibrium with Its Vapor, *J. Am. Chem. Soc. 72*, 2844−2847.
37. Andricioaei, I., and Karplus, M. (2001) On the calculation of entropy from covariance matrices of the atomic fluctuations, *J. Chem. Phys. 115*, 6289−6292.
38. Karplus, M., and Kushick, J. N. (1981) Method for Estimating the Configurational Entropy of Macromolecules, *Macromolecules 14*, 325−332.
39. Gomez, J., Hilser, V. J., Xie, D., and Freire, E. (1995) The Heat Capacity of Proteins, *Proteins 22*, 404−412.
40. Caflisch, A., and Karplus, M. (1994) Molecular Dynamics Simulation of Protein Denaturation: Solvation of the Hydrophobic Cores and Secondary Structure of Barnase, *Proc. Natl. Acad. Sci. U.S.A. 91*, 1746−1750.
41. Caflisch, A., and Karplus, M. (1995) Acid and Thermal Denaturation of Barnase Investigated by Molecular-Dynamics Simulations, *J. Mol. Biol. 252*, 672−708.
42. Hunenberger, P. H., Mark, A. E., and Vangunsteren, W. F. (1995) Computational Approaches to Study Protein Unfolding: Hen Egg-White Lysozyme as a Case Study, *Proteins 21*, 196−213.
43. Li, A. J., and Daggett, V. (1998) Molecular dynamics simulation of the unfolding of barnase: Characterization of the major intermediate, *J. Mol. Biol. 275*, 677−694.
44. Lounnas, V., and Wade, R. C. (1997) Exceptionally stable salt bridges in cytochrome P450cam have functional roles, *Biochemistry 36*, 5402−5417.
45. Dominy, B. N., Minoux, H., and Brooks, C. L. (2004) An electrostatic basis for the stability of thermophilic proteins, *Proteins: Struct., Funct., Bioinf. 57*, 128−141.
46. Robic, S., Guzman-Casado, M., Sanchez-Ruiz, J. M., and Marqusee, S. (2003) Role of residual structure in the unfolded state of a thermophilic protein, *Proc. Natl. Acad. Sci. U.S.A. 100*, 11345−11349.
47. Makhatadze, G. I., and Privalov, P. L. (1990) Heat Capacity of Proteins. 1. Partial Molar Heat Capacity of Individual Amino Acid Residues in Aqueous Solution: Hydration Effect, *J. Mol. Biol. 213*, 375−384.
48. Myers, J. K., Pace, C. N., and Scholtz, J. M. (1995) Denaturant M-Values and Heat-Capacity Changes: Relation to Changes in Accessible Surface Areas of Protein Unfolding, *Protein Sci. 4*, 2138−2148.

BI7004398